

Quantum dynamics of one and two bosonic atoms in a combined tight-binding periodic and weak parabolic potential

Manuel Valiente and David Petrosyan

Institute of Electronic Structure & Laser, FORTH, 71110 Heraklion, Crete, Greece

(Dated: June 7, 2021)

Strongly interacting bosonic particles in a tight-binding periodic potential superimposed by a weak parabolic trap is a paradigm for many cold atom experiments. Here, after revisiting the single particle problem, we study interaction-bound dimers of bosonic atoms in the combined lattice and parabolic potential. We consider both repulsively- and attractively-bound dimers and find pronounced differences in their behaviour. We identify conditions under which attractive and repulsive dimers exhibit analogous dynamics. Our studies reveal that coherent transport and periodic oscillations of appropriately prepared one- and two-atom wavepackets can be achieved, which may facilitate information transfer in optical lattice based quantum computation schemes.

PACS numbers: 03.75.Lm, 37.10.Jk, 03.65.Ge

I. INTRODUCTION

Quantum transport in periodic structures is one of the central topics of condensed matter physics [1]. Recent interest towards spatially-periodic systems has been largely motivated by the remarkable progress in cooling and trapping bosonic and fermionic atoms in optical lattices [2]. The relevant parameters of these systems can be controlled with very high precision and can be tuned to implement some of the fundamental models of condensed matter physics. In a tight-binding regime, the Hubbard model accurately describes static and dynamic properties of these systems [2, 3]. Importantly, in real experiments with cold atoms, the lattice is finite and often it is superimposed by a weak harmonic trap. This breaks the translational invariance of the lattice and thereby strongly modifies the properties of the system even in the limit of non-interacting particles [4, 5, 6]. In particular, the low energy states of the single-particle spectrum behave like harmonic oscillator states while the higher energy states are localized at the sides of the parabolic trap, which can lead to inhibition of quantum transport and dipole oscillations in a degenerate atomic gas [6, 7, 8, 9].

Atom-atom interactions profoundly enrich the Hubbard model, as attested by, e.g., theoretical prediction followed by spectacular experimental demonstration of the transition from the superfluid to the Mott insulator phase in an ensemble of cold bosonic atoms in optical lattice [10]. Strongly interacting bosons in periodic potentials can form tightly bound “dimers” [11] observed in a recent experiment [12] with repulsively interacting atoms in a lattice. Here we first discuss static and dynamic properties of a single atom in a combined periodic and weak parabolic potential and show that coherent transport and perfectly periodic oscillations of appropriately prepared wavepackets can be achieved. We then study the properties of strongly interacting atom pairs examining both regimes of attractive as well as repulsive interactions. We show that, quite generally, the interaction-bound dimers behave as single particles with appropriately rescaled parameters of the system. We iden-

tify, however, important differences between attractively-bound and repulsively-bound dimers and find, rather surprisingly, that, in a weak trap, the repulsive dimer is bound stronger than the attractive one.

II. THE MODEL

We consider cold bosonic atoms in a combined tight-binding periodic and weak parabolic potential. In 1D, the system is described by the Bose-Hubbard Hamiltonian

$$H = \sum_j \left[\Omega j^2 \hat{n}_j + \frac{U}{2} \hat{n}_j (\hat{n}_j - 1) - J (b_j^\dagger b_{j+1} + b_{j+1}^\dagger b_j) \right], \quad (1)$$

where b_j^\dagger (b_j) is the creation (annihilation) operator and $\hat{n}_j = b_j^\dagger b_j$ the number operator for site j , J is the tunnel coupling between adjacent sites, U is the on-site interaction, and $\Omega > 0$ quantifies the strength of the superimposed parabolic potential due to which site $j = \pm 1, \pm 2, \dots$ acquires energy offset Ωj^2 with respect to site $j = 0$ corresponding to the minimum of the potential. A natural basis for Hamiltonian (1) is that of the eigenstates $|n_j\rangle \equiv \frac{1}{\sqrt{n!}} (b_j^\dagger)^n |0\rangle$ of operator \hat{n}_j whose eigenvalues $n = 0, 1, 2, \dots$ denote the number of particles at site j , and $|0\rangle \equiv |\{0_j\}\rangle$ is the vacuum state.

Single particle spectrum. We first discuss the single-particle case with the on-site interaction U playing no role. Recall that in the absence of parabolic potential, $\Omega = 0$, the eigenstates of the Hubbard Hamiltonian (1) form a Bloch band of width $4J$ centered around zero. More quantitatively, given a finite flat lattice of \bar{N} sites, the Bloch eigenenergies and corresponding eigenstates are given by

$$\bar{E}_k = -2J \cos \left[\frac{\pi(k+1)}{\bar{N}+1} \right], \quad (2a)$$

$$|\bar{\chi}_k\rangle = \mathcal{N} \sum_{l=1}^{\bar{N}} \sin \left[\frac{l\pi(k+1)}{\bar{N}+1} \right] |1_l\rangle, \quad (2b)$$

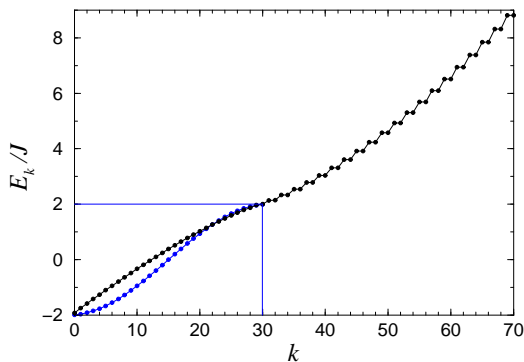


FIG. 1: Single particle energy eigenvalues E_k in a combined periodic and parabolic potential obtained by numerical diagonalization of Hamiltonian (1) with $J/\Omega = 140$. For comparison, the blue dots represent eigenvalues \bar{E}_k within the Bloch (mini)band for a flat lattice ($\Omega = 0$) of length $\bar{N} = N = 31$.

with $0 \leq k < \bar{N}$ and \mathcal{N} a normalization constant. In the limit of $\bar{N} \rightarrow \infty$, Eq. (2a) yields the well-known dispersion relation [1] $\bar{E}_q = -2J \cos(q)$ with $0 \leq q \leq \pi$ and lattice constant $d = 1$. Remarkably, however, even a very weak parabolic potential $\Omega \ll J$ drastically modifies the spectrum of Hamiltonian (1) [4, 5], as shown in Fig. 1. Note that the spectrum, bound from below by $-2J$, is composed of discrete energy levels E_k . Two distinct groups of levels can be identified: (i) the low-energy levels $E_k \leq 2J$ forming a modified Bloch band, and (ii) the high-energy ones $E_k > 2J$.

(i) The parabolic potential effectively restricts the number of sites accessible to a particle with energy within the Bloch band $-2J \leq E_k \leq 2J$. Roughly, only sites $j = 0, \pm 1, \dots$, for which $\Omega j^2 < 2J$, can participate in the formation of the low-energy part of the spectrum [5]. More precisely, using second order perturbative corrections, we find that the modified Bloch band is restricted to sites j satisfying

$$|j| \leq j_{\max} \equiv \sqrt{\left(1 + \frac{1}{\sqrt{2}}\right) \frac{J}{\Omega}} \simeq 1.3 \sqrt{\frac{J}{\Omega}}. \quad (3)$$

The low-energy part of the spectrum therefore contains $N = 2\lfloor j_{\max} \rfloor + 1$ energy levels E_0, E_1, \dots, E_{N-1} , which is illustrated in Fig. 1, and we have verified this conclusion for a wide range of values of J/Ω . Note that the weak parabolic potential modifies the Bloch band in such a way that its lowest energy part is approximately linear in k , similar to the spectrum of a harmonic oscillator. Indeed, using the properties of the Mathieu functions [13], it can be shown [5] that in the limit of $J/\Omega \gg 1$, the low-energy eigenvalues E_k and eigenstates $|\chi_k\rangle$ of Hamiltonian (1) are well approximated by

$$E_k \approx -2J + 2\sqrt{J\Omega} \left(k + \frac{1}{2}\right), \quad (4a)$$

$$|\chi_k\rangle \approx \mathcal{N} \sum_j (2^k k!)^{-1/2} e^{-\zeta_j^2/2} H_k(\zeta_j) |1_j\rangle, \quad (4b)$$

where \mathcal{N} is a normalization constant, $\zeta_j = j\sqrt{4\Omega/J}$ is the discretized coordinate, and $H_k(\zeta)$ is the k -th Hermite polynomial. Thus, the lowest energy eigenvalues E_k and eigenstates $|\chi_k\rangle$ correspond to those of an energy-shifted harmonic oscillator with an effective frequency $\hbar\omega = 2\sqrt{J\Omega}$ and an effective mass given by the usual expression $\mu = \hbar^2/(2Jd^2)$ [1] which is valid near the bottom of the lowest Bloch band of a periodic potential. In particular, the ground state with $E_0 = -2J + \sqrt{J\Omega}$ is given by

$$|\chi_0\rangle = \sqrt{\frac{\Omega}{\pi^2 J}} \sum_j e^{-\zeta_j^2/2} |1_j\rangle. \quad (5)$$

The spectrum at the top of the modified Bloch band approaches that of a uniform ($\Omega = 0$) finite ($\bar{N} = N$) lattice given by Eq. (2a).

(ii) On the other hand, the high-energy eigenvalues $E_k > 2J$ with $k \geq N$ are two-fold degenerate, as seen in Fig. 1. The pairs of degenerate states with indices $k = 2|j| + 1$ and $k' = 2|j| + 2$ are localised around sites $j = \pm|j|$ ($|j| > j_{\max}$) equidistant from the center of the parabolic potential, the corresponding energies being given by $E_{k,k'} \approx \Omega j^2$ [4, 5]. For such states, the localization occurs because, for large enough $|j|$, the transitions $|1_j\rangle \rightarrow |1_{j\pm 1}\rangle$ effected by the last term of Hamiltonian (1) become non-resonant and the particle tunneling between neighboring lattice sites is suppressed. These high-energy states were shown to be responsible for damping of dipole oscillations and quantum transport of degenerate atomic gases in combined harmonic and optical lattice potentials [5, 6, 7, 8, 9]. Such localised states can be selectively addressed by radio-frequency fields [14] and may be employed for efficient initialization of a qubit register with fermionic atoms [15].

Coherent dynamics of a single particle wavepacket. From the above analysis, it is clear that if we restrict ourselves to the harmonic oscillator-like states belonging to the lowest part of the energy spectrum, we can expect a quasi-periodic dynamics in the system. Non-dispersive transport of a single particle wavepacket from one side of the shallow parabolic potential to the other can then be achieved. In Fig. 2(a) we show the dynamics of a single particle wavepacket $|\psi\rangle$, represented by the ground state of the system $|\chi_0\rangle$, Eq. (5), initially shifted by 7 sites from the trap center. Numerical solution of the Schrödinger equation using Hamiltonian (1) reveals almost perfect periodic oscillations of the discrete Gaussian wavepacket between the two sides of the parabolic potential with period $\tau \simeq 2\pi/\omega = (\pi\hbar/J)\sqrt{J/\Omega}$.

From the set of harmonic oscillator-like states $|\chi_k\rangle$ of Eq. (4b), we can construct a well-localized wavepacket $|\psi^{(j')}\rangle$ centered at a prescribed site j' ($|j'| < j_{\max}$). If we write the initial state as

$$|\psi(0)\rangle = \sum_k A_k |\chi_k\rangle, \quad (6)$$

the probability amplitude a_j for a particle to be at site j

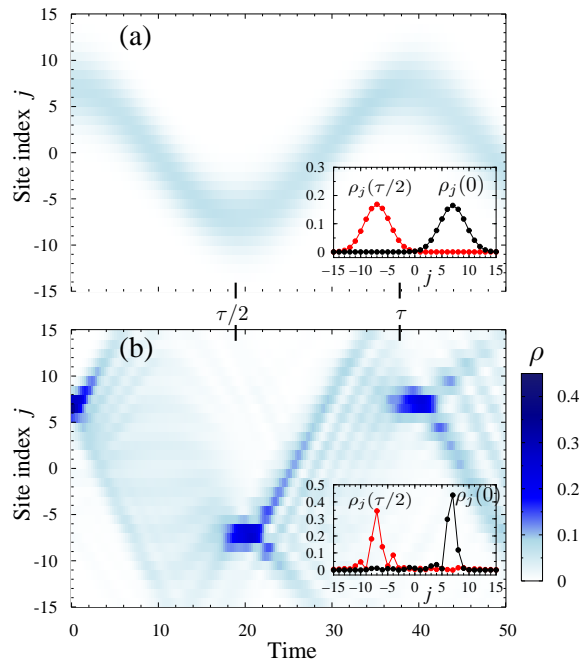


FIG. 2: Time evolution of density $\rho_j \equiv \langle \hat{n}_j \rangle$ for a single particle wavepacket $|\psi\rangle$ in a combined periodic and parabolic potential with $J/\Omega = 140$. (a) Initial state $|\psi(0)\rangle$ corresponds to the ground state $|\chi_0\rangle$ (discrete Gaussian) shifted by 7 sites from the trap center. (b) Initial state $|\psi^{(j')}(0)\rangle$ is a localized around $j' = 7$ wavepacket constructed from the $k = 0, 1, \dots, 20$ eigenstates $|\chi_k\rangle$. Insets in (a) and (b) show the density distribution ρ_j at $t = 0$ and $t \simeq \tau/2$. Time is measured in units of $\hbar J^{-1}$.

is given by

$$a_j = \langle 1_j | \psi(0) \rangle \propto \sum_k A_k (2^k k!)^{-1/2} e^{-\zeta_j^2/2} H_k(\zeta_j). \quad (7)$$

To obtain a localized around site j' state $|\psi^{(j')}\rangle$, we maximize $|a_{j'}|^2$, which determines the set of coefficients $\{A_k\}$ in Eq. (6). In Fig. 2(b) we show the time evolution of such a localized state, which exhibits periodic collapses and partial revivals at sites $-j'$ and j' with time steps $\tau/2$. The revivals are not complete since, as noticed above, the energy spectrum E_k for small k is only approximately linear in k . Nevertheless, our results suggest that coherent non-dispersive transport of carefully engineered atomic wavepackets can be achieved in optical lattices in the presence of a shallow parabolic potential.

III. TWO PARTICLE DYNAMICS

We now consider two bosonic particles in the combined periodic and weak parabolic potential. Clearly, in the simplest case of feeble interaction $|U| \ll J$, we have two independent particles for which the results of the previous section apply. But even for strong on-site interaction U , some aspects of the combined dynamics of two low-

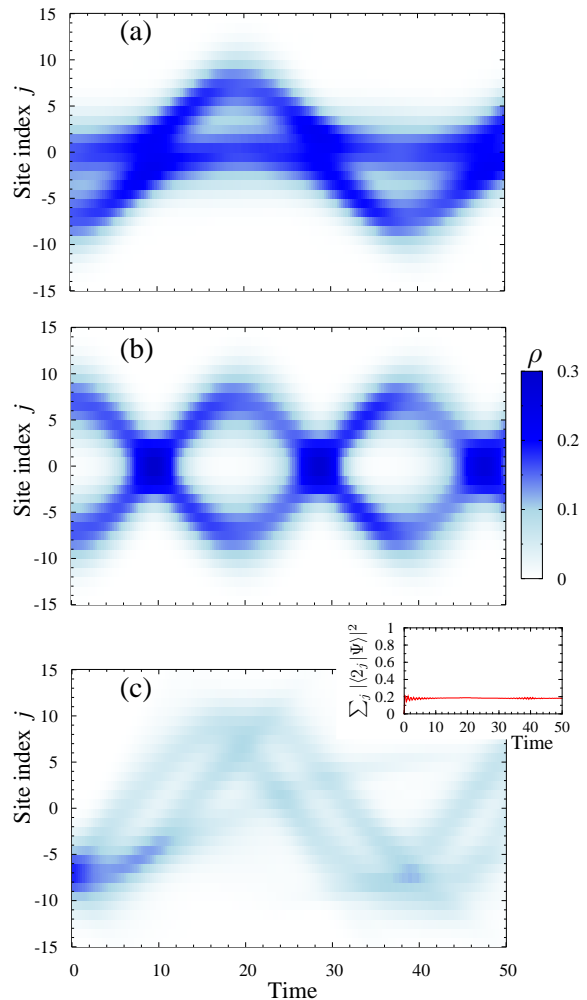


FIG. 3: Time evolution of density $\rho_j \equiv \langle \hat{n}_j \rangle$ for two particles in a combined periodic and parabolic potential with $J/\Omega = 140$ and $U = -10J$. (a) Initial state $|\Psi(0)\rangle$ corresponds to one particle in the ground state $|\chi_0\rangle$ and the other particle in state $|\chi_0\rangle$ shifted from the trap center by 7 sites. (b) Initially both particles in state $|\chi_0\rangle$ are shifted from the trap center by 7 sites in opposite directions. (c) Initial state corresponds to both particles in state $|\chi_0\rangle$ shifted from the trap center by 7 sites in the same direction. Inset in (c) shows the projection $\sum_j |\langle 2_j | \Psi \rangle|^2$.

energy particles can be inferred from the independent particle picture modified by short-range collisions. This applies when the initial state $|\Psi(0)\rangle = |\psi\rangle \otimes |\psi'\rangle$ is composed of two non-overlapping single-particle wavepackets, $|\langle \psi | \psi' \rangle|^2 \ll 1$, which upon collision with each other are reflected by the potential barrier $|U| \gtrsim J$. Examples of such a situation with large on-site attractive interaction energy $U = -10J$ are shown in Figs. 3(a) and 3(b). Analogous dynamics is observed for the repulsive interaction $U = 10J$.

More intriguing is the case of initial state $|\Psi(0)\rangle = |\psi\rangle \otimes |\psi\rangle$ consisting of two overlapping single-particle wavepackets shown in Fig. 3(c). This state has a signif-

icant population of the two-particle states $|2_j\rangle$ given by $\sum_j |\langle 2_j | \Psi \rangle|^2 \simeq \sum_j |a_j|^4$, where a_j are the single-particle probability amplitudes. Clearly, the population of two-particle states is largest in the central part of the initial density distribution. As seen in Fig. 3(c), this part exhibits slow dynamics, characterized by the effective tunnelling constant $J^{(2)} = -2J^2/U$ (see below), and separates from the wings of the initial density profile. The wings, formed by the single-particle states $|1_j\rangle$, oscillate between the two sides of parabolic potential with the usual period τ .

Interaction-bound dimers. At this point, let us recall [11, 12] that two bosonic particles occupying the same site j can form an effective ‘‘dimer’’ bound by the on-site interaction U . Thus, when $|U| \gg J$, the first-order transitions $|2_j\rangle \rightarrow |1_j\rangle |1_{j\pm 1}\rangle$ effected by the last term of Hamiltonian (1) are non-resonant and the particles can not separate. However, the second-order in J transitions $|2_j\rangle \rightarrow |2_{j\pm 1}\rangle$ via virtual intermediate states $|1_j\rangle |1_{j\pm 1}\rangle$ are resonant. Consequently, the dimer can tunnel as a whole with the effective rate $J^{(2)} = -2J^2/U \ll J$ [11]. This explains the dynamics seen in Fig. 3(c) where the initial density distribution splits into slow and fast propagating components, the former composed of the dimer states $|2_j\rangle$ while the latter containing the monomer states $|1_j\rangle$.

If the initial state is prepared in such a way that only two-particle (dimer) states are populated, as implemented in, e.g., [12], for $|U| \gg J$ the system can, to a good approximation, be described by an effective dimer Hamiltonian derived in the second order in J/U [11]. In terms of the dimer creation $c_j^\dagger = (b_j^\dagger)^2 [1/\sqrt{2(\hat{n}_j + 1)}]$ and annihilation $c_j = [1/\sqrt{2(\hat{n}_j + 1)}] (b_j)^\dagger$ operators, and number operator $\hat{m}_j = c_j^\dagger c_j = \hat{n}_j/2$, the effective Hamiltonian for a single dimer reads [16]

$$H_{\text{eff}} = \sum_j \left[\Omega^{(2)} j^2 \hat{m}_j + (U - J^{(2)}) \hat{m}_j - J^{(2)} (c_j^\dagger c_{j+1} + c_{j+1}^\dagger c_j) \right], \quad (8)$$

where $\Omega^{(2)} = 2\Omega$ is the strength of a parabolic potential seen by the dimer, while $(U - J^{(2)})$ represents the ‘‘internal’’ energy of a dimer.

Before proceeding, let us note that, differently from the flat lattice situation considered in [11], here the effective Hamiltonian H_{eff} is not applicable in the vicinity of sites $|j| \simeq |U|/(2\Omega)$ where near-resonant dissociation of a dimer can occur via transitions $|2_j\rangle \rightarrow |1_j\rangle |1_{j\pm 1}\rangle$. But since we are interested in the dynamics of low-energy dimers with $|U| \gg J \gg \Omega$, such high- j states cannot be reached.

Consider first the case of strong attractive interaction $U < 0$ leading to a positive tunnelling constant $J^{(2)} > 0$. Then the effective Hamiltonian (8) has the same form as the Hubbard Hamiltonian (1) for a single particle in a combined periodic and parabolic potential. We can therefore immediately write the lowest energy eigenvalues

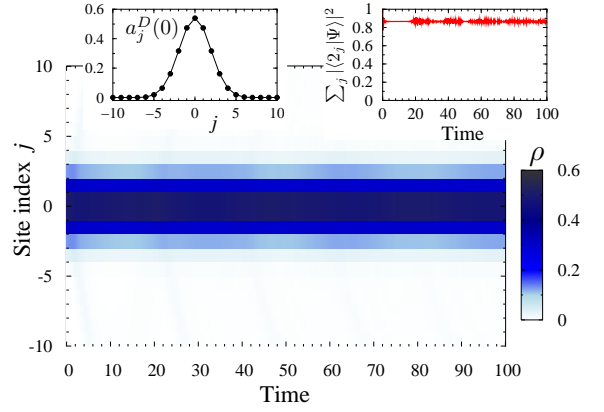


FIG. 4: Time evolution of atom density $\rho_j \equiv \langle \hat{n}_j \rangle$ for an attractively-bound dimer in a combined periodic and parabolic potential with $J/\Omega = 140$ and $U = -10J$. Initial state $|\Psi(0)\rangle$ corresponds to the ground state $|\chi_0^D\rangle$ of the effective Hamiltonian (8) with the dimer amplitudes $a_j^D(0)$ shown in the left inset. Right inset is the projection $\sum_j |\langle 2_j | \Psi \rangle|^2$.

and eigenstates for an effective dimer as

$$E_k^D \approx -2J^{(2)} + 2\sqrt{J^{(2)}\Omega^{(2)}} \left(k + \frac{1}{2}\right), \quad (9a)$$

$$|\chi_k^D\rangle \approx \mathcal{N} \sum_j (2^k k!)^{-1/2} e^{-\xi_j^2/2} H_k(\xi_j) |1_j^D\rangle, \quad (9b)$$

where energies E_k^D are relative to the dimer internal energy $(U - J^{(2)})$, $\xi_j = j^4 \sqrt{\Omega^{(2)}/J^{(2)}} = j^4 \sqrt{\Omega|U|/J^2}$ is the discrete coordinate, and $|1_j^D\rangle \equiv c_j^\dagger |0\rangle$ denotes a state with a single dimer at site j ; obviously $|1_j^D\rangle = |2_j\rangle$. The modified Bloch band $-2J^{(2)} \leq E_k^D \leq 2J^{(2)}$ for the dimer is restricted to the sites with

$$|j| \leq j_{\text{max}}^D \equiv \sqrt{\left(1 + \frac{1}{\sqrt{2}}\right) \frac{J^{(2)}}{\Omega^{(2)}}} \simeq 1.3 \sqrt{\frac{J}{\Omega} \frac{J}{|U|}}, \quad (10)$$

thus containing $N^D = 2\lfloor j_{\text{max}}^D \rfloor + 1$ energy levels E_k^D with $0 \leq k < N^D$. The effective harmonic oscillator frequency at the bottom of the modified Bloch band is $\hbar\omega^D = 2\sqrt{J^{(2)}\Omega^{(2)}}$ and the dimer effective mass $\mu^D = \hbar^2/(2J^{(2)}d^2)$ is large ($J^{(2)} \ll J$) and positive. We have verified these conclusions by numerically solving the Schrödinger equation using the exact Hamiltonian (1) with the initial conditions corresponding to eigenstates (9b) of the effective Hamiltonian (8). As an example, in Fig. 4 we show the time evolution, or nearly complete absence thereof, of the system in the ground state of (8),

$$|\chi_0^D\rangle \simeq \sqrt{\frac{\Omega^{(2)}}{\pi^2 J^{(2)}}} \sum_j e^{-\xi_j^2/2} |1_j^D\rangle = \sqrt{\frac{\Omega|U|}{\pi^2 J^2}} \sum_j e^{-\xi_j^2/2} |2_j\rangle, \quad (11)$$

with energy $E_0^D = -2J^{(2)} + \sqrt{J^{(2)}\Omega^{(2)}}$.

We next turn to the case of strong repulsive interaction $U > 0$. The dimer tunneling constant is negative,

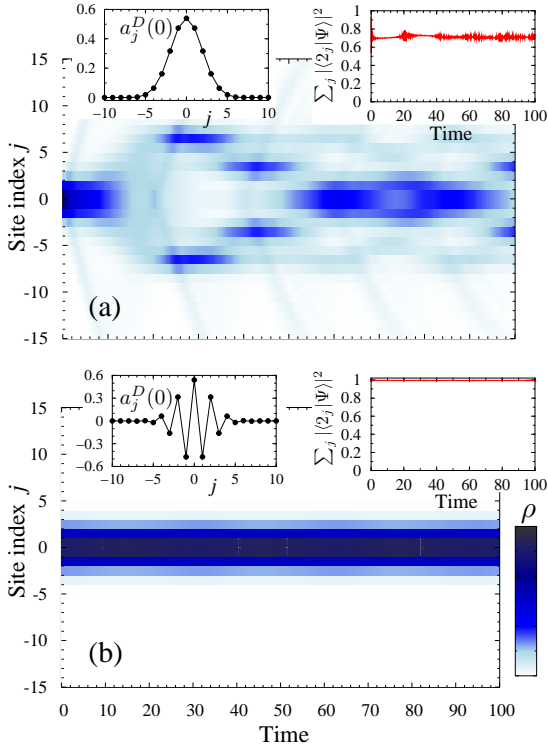


FIG. 5: Time evolution of density $\rho_j \equiv \langle \hat{n}_j \rangle$ for repulsively-bound dimer in a combined periodic and parabolic potential with $J/\Omega = 140$ and $U = 10J$. (a) Initial state $|\Psi(0)\rangle$ is the ground state $|\chi_0^D\rangle$ of attractive dimer, Eq. (11), with amplitudes $a_j^D(0)$ shown in the left inset. (b) Initial state $|\Psi(0)\rangle$ is the ground state $|\tilde{\chi}_0^D\rangle$ of repulsive dimer, Eq. (14), with amplitudes $a_j^D(0)$ shown in the left inset. Right insets are the projections $\sum_j |\langle 2_j | \Psi \rangle|^2$.

$J^{(2)} < 0$, corresponding to a negative effective mass μ^D [11]. As a result, $|\chi_0^D\rangle$ in Eq. (11) is no longer the ground state of Hamiltonian (8), as attested in Fig. 5(a). Rather, it is a highly excited state. To see this, consider for a moment a single particle in a flat lattice of \bar{N} sites with $J < 0$. It follows from Eqs. (2a), (2b) that the lowest energy state with $\bar{E}_{\bar{N}-1} = -2J \cos[\pi/(\bar{N}+1)] = -2|J| \cos[\pi/(\bar{N}+1)]$ is

$$|\bar{\chi}_{\bar{N}-1}\rangle = -\mathcal{N} \sum_{l=1}^{\bar{N}} \sin \left[\frac{l\pi}{\bar{N}+1} \right] e^{il\pi} |1_l\rangle. \quad (12)$$

Thus, in the limit of infinite lattice $\bar{N} \rightarrow \infty$, the ground state corresponds to the Bloch wave with quasi-momentum $q = \pi$. Returning back to the repulsively-bound dimer in the combined periodic and parabolic potential, we find that the low-energy eigenvalues are those of Eq. (9a) with the replacement $J^{(2)} \rightarrow |J^{(2)}|$, while the corresponding eigenstates are given by

$$|\tilde{\chi}_k^D\rangle \approx \mathcal{N} \sum_j (2^k k!)^{-1/2} e^{-\xi_j^2/2} H_k(\xi_j) e^{i\pi j} |1_j^D\rangle. \quad (13)$$

The ground state with $E_0^D = -2|J^{(2)}| + \sqrt{|J^{(2)}|\Omega^{(2)}}$ is

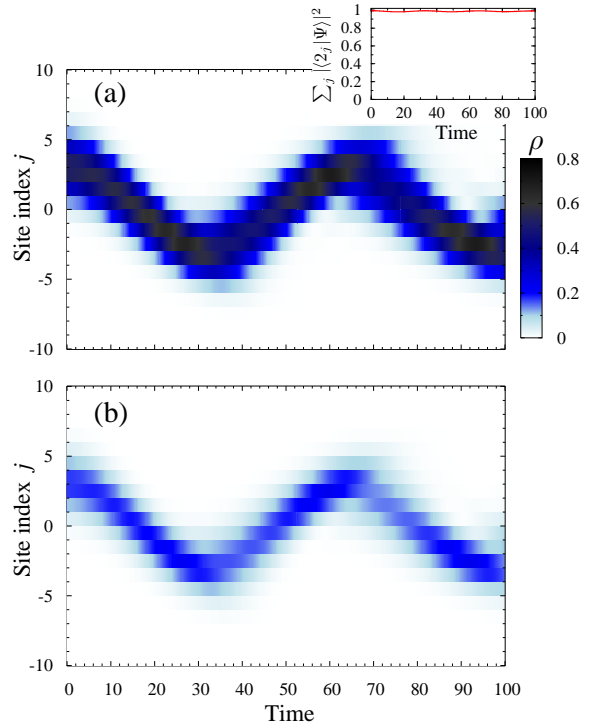


FIG. 6: Time evolution of (a) atom density $\rho_j \equiv \langle \hat{n}_j \rangle$, and (b) dimer density $\rho_j^D \equiv \langle \hat{m}_j \rangle \simeq \rho_j/2$ in a combined periodic and parabolic potential with $J/\Omega = 140$ and $U = 10J$. Initial state $|\Psi(0)\rangle$ corresponds to the dimer ground state $|\tilde{\chi}_0^D\rangle$ shifted by 3 sites from the trap center. (a) is the numerical solution of the Schrödinger equation with the exact Hamiltonian (1), while (b) is obtained with the effective Hamiltonian (8). Inset in (a) is the projections $\sum_j |\langle 2_j | \Psi \rangle|^2$.

then

$$\begin{aligned} |\tilde{\chi}_0^D\rangle &\simeq \sqrt{\frac{\Omega^{(2)}}{\pi^2 |J^{(2)}|}} \sum_j e^{-\xi_j^2/2} e^{i\pi j} |1_j^D\rangle \\ &= \sqrt{\frac{\Omega |U|}{\pi^2 J^2}} \sum_j e^{-\xi_j^2/2} (-1)^j |2_j\rangle, \end{aligned} \quad (14)$$

which is confirmed by our numerical simulations illustrated in Fig. 5(b). Remarkably, the repulsive dimer appears to be tighter bound than the attractive one. The symmetry between the cases of $U < 0$ and $U > 0$ is broken due to the presence of a parabolic potential.

Finally, in Fig. 6 we show the dynamics of a dimer wavepacket $|\Psi\rangle$, represented by the ground state $|\tilde{\chi}_0^D\rangle$ initially shifted by 3 sites from the trap center (for these parameters, $j_{\max}^D \simeq 4.9$). Our simulations using the exact Hamiltonian (1) and the effective Hamiltonian (8) yield practically identical results, which amount to periodic oscillations of the dimer wavepacket between the two sides of parabolic potential with period $\tau^D \simeq 2\pi/\omega^D = (\pi\hbar/2J)\sqrt{U/\Omega}$. Numerical simulations for attractively bound dimers reveal similar behaviour but with considerably larger admixture of the single-particle states,

$\sum_j |\langle 1_j | \Psi \rangle|^2 \lesssim 0.2$. This is another manifestation of the fact that the repulsive dimer in a combined periodic and weak parabolic potential is bound tighter than the attractive dimer under the otherwise similar conditions.

IV. CONCLUSIONS

To summarize, in this paper we have studied coherent quantum dynamics of one and two bosonic particles in a combined tight-binding periodic and shallow parabolic potential. Our studies are relevant to current experiments with cold alkali atoms in optical lattices and weak magnetic (or optical) traps [2]. After revisiting the single-particle problem, we considered effective interaction-bound dimers recently realized in the experiment [12] with strong repulsive atom-atom interactions. We examined both cases of repulsively-bound and attractively-bound dimers and identified similarities

as well as marked differences in their static and dynamic properties. In particular, a rather counterintuitive feature of the system revealed by the present work was that the repulsive dimers are bound stronger than the attractive dimers, as far as their ground states and coherent dynamics associated with low-energy states is concerned. In addition, we have shown that non-dispersive transport of carefully prepared atomic wavepackets can be achieved. As an extension of the present work, we plan to study dimer–monomer resonant collisions and entanglement of the resulting wavepackets. Our results may be pertinent to quantum information schemes with cold atoms in optical lattices.

Acknowledgments

This work was supported by the EC Marie-Curie Research Training Network EMALI.

-
- [1] N.J. Ashcroft and N.D. Mermin, *Solid State Physics* (International Thomson Publishing, New York, 1976).
- [2] O. Morsch and M. Oberthaler, *Rev. Mod. Phys.* **78**, 179 (2006); I. Bloch, *J. Phys. B* **38**, S629 (2005).
- [3] D. Jaksch and P. Zoller, *Ann. Phys. (N.Y.)* **315**, 52 (2005).
- [4] C. Hooley and J. Quintanilla, *Phys. Rev. Lett.* **93**, 080404 (2004).
- [5] A.M. Rey, G. Pupillo, C.W. Clark, and C.J. Williams, *Phys. Rev. A* **72**, 033616 (2005).
- [6] M. Rigol and A. Muramatsu, *Phys. Rev. A* **70**, 043627 (2004).
- [7] V. Ruuska and P. Törmä, *New J. Phys.* **6**, 59 (2004).
- [8] L. Pezze, L. Pitaevskii, A. Smerzi, S. Stringari, G. Modugno, E. de Mirandes, F. Ferlaino, H. Ott, G. Roati, and M. Inguscio, *Phys. Rev. Lett.* **93**, 120401 (2004).
- [9] C.D. Fertig, K.M. O’Hara, J.H. Huckans, S.L. Rolston, W.D. Phillips, and J.V. Porto, *Phys. Rev. Lett.* **94**, 120403 (2005).
- [10] D. Jaksch, C. Bruder, J.I. Cirac, C.W. Gardiner, and P. Zoller, *Phys. Rev. Lett.* **81**, 3108 (1998); M. Greiner, O. Mandel, T. Esslinger, T.W. Hänsch, and I. Bloch, *Nature* **415**, 39 (2002).
- [11] D. Petrosyan, B. Schmidt, J.R. Anglin, and M. Fleischhauer, *Phys. Rev. A* **76**, 033606 (2007).
- [12] K. Winkler, G. Thalhammer, F. Lang, R. Grimm, J. Hecker Denschlag, A.J. Daley, A. Kantian, H.P. Büchler, and P. Zoller, *Nature* **441**, 853 (2006).
- [13] M. Abramowitz and I. Stegun, *Handbook of Mathematical Functions* (Dover Publications, New York, 1965).
- [14] H. Ott, E. de Mirandes, F. Ferlaino, G. Roati, V. Türec, G. Modugno, and M. Inguscio, *Phys. Rev. Lett.* **93**, 120407 (2004).
- [15] L. Viverit, C. Menotti, T. Calarco, and A. Smerzi, *Phys. Rev. Lett.* **93**, 110401 (2004).
- [16] For the sake of convenience, here the sign of the dimer tunnel coupling $J^{(2)} = -2J^2/U$ is taken opposite to that in [11], while the nearest neighbour interaction does not play a role since we consider only a single dimer in the system.